Progress In Electromagnetics Research M, Vol. 97, 119–131, 2020

Low SLL Pattern of Elliptical Aperture Array Based on Innovative Optimization Method

Amirsaman Zare*

Abstract—An elliptical array composed of 10 uniform elliptical apertures as the radiating elements is presented. Assume that each aperture in an electric conducting plane spreads on the elliptic orbit and is fed by the uniform plane wave in order to obtain a low SLL array pattern with high directivity. The elliptic orbit eccentricity and the angular position of each array element are stimulated. The applied parameters are determined by an elaborate optimization procedure. The utilized procedure comprising the geometric computational technique (GCT), and angular positions excitation (APE) is stated in detail, respectively to determine a satisfactory eccentricity and the angular position of each element.

1. INTRODUCTION

Antenna array is required for the present era of wireless communications and a great choice to use in enormous range of electromagnetic applications [2, 4, 8]. The utilization aspect of antenna arrays has been rapidly developed to attract the advantages of capacity enhancement in communication systems, where an essential structure of antenna arrays with an optimized radiation pattern is demanded [9, 10, 15, 19, 20]. The production of the desired radiation pattern requests various techniques to achieve the best outcome [4, 6, 8–12]. To address these utilized optimization techniques, several methods have been used in [3–18], whose target is the modifications in the antenna array parameters to attain the best radiation pattern [4, 6, 7–12]. Variations in array radiating elements facilitate the way to obtain better radiation characteristics [11, 12, 16]. The preference of aperture antennas used in array structures is associated with the advantages of suitable integration to telecommunication devices and also notable interaction between the antenna pattern characteristics [1, 2, 5]. In this work, an elliptical array of 10 uniform elliptical apertures is introduced. The antenna array function is studied to produce the radiation pattern, while apertures electric field respectively is x and y-directed. For elliptical array pattern, the eccentricity is a significant controlling component.

The acceleration in process of SLL reduction and directivity enhancement is a desired consequence to modify the eccentricity and angular position value [2]. The paper proposes the geometric computational technique (GCT) to adjust the eccentricity and APE manner explained as follows. Two concentric ellipses, within each of which one rectangle is inscribed, are assumed. Both the ellipses are increased to more concentric intersecting ellipses with the same geometric characteristics. The sequence of rectangles inside the concentric intersecting ellipses in the oval areas yields two polygon shapes. The obtained equation through the area of the space between two polygons in the supposed geometric diagram is an expression multiplied by the semi-major and semi-minor axes subsequently to result in the optimal eccentricity amount. The APE is utilized to vary the angular positions, if the best radiation pattern is not attained by eccentricity excitation. The paper continues in following sections. Section 2 introduces antenna array configuration and its formulations. In Section 3, an overview of optimization method and numerical results with comparisons are provided. The conclusion is given in Section 4.

Received 24 March 2020, Accepted 16 April 2020, Scheduled 12 October 2020
* Corresponding author: Amirsaman Zare (amirsaman1989@gmail.com).
The author is with the TU Darmstadt, Germany.

2. ANTENNA ARRAY CONFIGURATION

This section is presented to consider an elliptical array of 10 uniform elliptical apertures set in the electric conducting plane and positioned on an elliptic orbit. An opening structure with elliptical figure and constant in amplitude distribution is known as the uniform elliptical aperture as shown in Fig. 1 [1, 3].

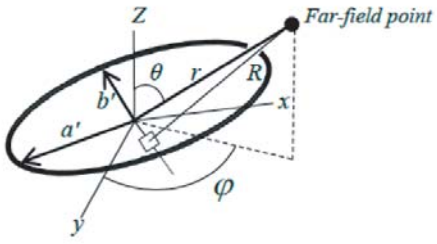

Figure 1. Elliptical aperture antenna.

Discuss the elliptical apertures in this article demonstrating the exodus holes of elliptical array with the major and minor axes $\acute{a}$ and $\acute{b}$. A generalized procedure finds the electric far field of a uniform elliptical aperture set in a conducting overview plane. The supposed aperture fields E_a and H_a applied by the physical optics approximations only exist over the aperture surface and are required to obtain the density of electric and magnetic equivalent surface currents by the following Equations (1) and (2) [1, 3].

$\hat{n}$ is the exterior normal vector on the aperture surface.

$$\vec{J}_s = \hat{n} \times \vec{H}_a \tag{1}$$

$$\vec{M}_s = \vec{E}_a \times \hat{n} \tag{2}$$

The aperture fields related to equivalent surface currents are affiliated with the vector potentials [1, 3].

$$\vec{A} = \mu \frac{e^{-j\beta r}}{4\pi r} \hat{n} \times \iint\limits_{Sa} \vec{H}_a e^{j\beta \hat{r}\acute{r}} d\acute{S} \tag{3}$$

$$\vec{F} = \varepsilon \frac{e^{-j\beta r}}{4\pi r} \hat{n} \times \iint\limits_{Sa} \vec{E}_a e^{j\beta \hat{r}\acute{r}} d\acute{S} \tag{4}$$

As given by Equations (3) and (4), $\vec{A}$ and $\vec{F}$ respectively are magnetic and electric vector potentials, and regarding to elliptical geometry, Sa is introduced as the aperture surface.

Pursuant to Equations (3) and (4), the vector potentials integrals contain two-dimensional Fourier transforms. Due to utilizing a more accurate procedure, the Fourier transforms cast in terms of Q and P are used to calculate an aperture radiating far-fields [1, 3].

$$Q = \iint\limits_{Sa} \vec{H}_a e^{j\beta \hat{r}\acute{r}} d\acute{S} \tag{5}$$

$$P = \iint\limits_{Sa} \vec{E}_a e^{j\beta \hat{r}\acute{r}} d\acute{S} \tag{6}$$

Equations (3)–(6) are simplified to Equations (7) and (8). To imply the aperture fields components in arbitrary directions, the terms of the Fourier transforms are demonstrated by their x and y-vector components, $\hat{n} = \hat{z}$.

$$\vec{A} = \mu \frac{e^{-j\beta r}}{4\pi r} (Q_x \hat{y} - Q_y \hat{x}) \tag{7}$$

$$\vec{F} = -\varepsilon \frac{e^{-j\beta r}}{4\pi r} (P_x \hat{y} - P_y \hat{x}) \tag{8}$$

Express x and y in spherical coordinates retained in φ and θ-components.

$$\vec{A} = \mu\frac{e^{-j\beta r}}{4\pi r}(\cos\theta(Q_x\sin\varphi - Q_y\cos\varphi)\hat{\theta} + (Q_x\cos\varphi + Q_y\sin\varphi)\hat{\varphi}) \tag{9}$$

$$\vec{F} = -\varepsilon\frac{e^{-j\beta r}}{4\pi r}(\cos\theta(P_x\sin\varphi - P_y\cos\varphi)\hat{\theta} + (P_x\cos\varphi + P_y\sin\varphi)\hat{\varphi}) \tag{10}$$

The electric far-field associated with the aperture fields and determined in terms of the vector potentials is expressed by the equations below [1, 3]. $\vec{r}$ is the unit vector in a spherical system.

$$\vec{E} = \vec{E}_A + \vec{E}_F \tag{11}$$

$$\vec{E} = -j\omega\vec{A} - j\omega\eta\vec{F}\times\vec{r} \tag{12}$$

The total electric far-field is in analogous style to Equations (9) and (10).

$$\begin{aligned}\vec{E} = {} & j\beta\frac{e^{-j\beta r}}{4\pi r}(\eta\cos\theta(Q_y\cos\varphi - Q_x\sin\varphi)\hat{\theta} - \eta(Q_y\sin\varphi + Q_x\cos\varphi)\hat{\varphi} \\ & +(P_y\sin\varphi + P_x\cos\varphi)\hat{\theta} + \cos\theta(P_y\cos\varphi - P_x\sin\varphi)\hat{\varphi})\end{aligned} \tag{13}$$

The electric far-field is obtained along the z axis in the right half space or $z > 0$ by the supposition that the aperture is in a perfect magnetic conducting plane [1, 3].

$$\vec{M}_s = 0 \Rightarrow \vec{E} = 2\vec{E_A}$$

$$\vec{E} = j\beta\eta\frac{e^{-j\beta r}}{2\pi r}(\cos\theta(Q_y\cos\varphi - Q_x\sin\varphi)\hat{\theta} - (Q_y\sin\varphi + Q_x\cos\varphi)\hat{\varphi}) \tag{14}$$

The electric far-field is obtained along the z axis in the right half space or $z > 0$ by the supposition that the aperture is in a perfect electric conducting plane [1, 3].

$$\vec{J}_s = 0 \Rightarrow \vec{E} = 2\vec{E_F}$$

$$\vec{E} = j\beta\frac{e^{-j\beta r}}{2\pi r}((P_y\sin\varphi + P_x\cos\varphi)\hat{\theta} + \cos\theta(P_y\cos\varphi - P_x\sin\varphi)\hat{\varphi}) \tag{15}$$

2.1. Uniform Elliptical Apertures Array

Exploit a great number of apertures in the different configuration types of arrays to generate a distinctive radiation pattern. The author studies and optimizes an elliptical array construction integrated with 10 uniform elliptical apertures as the radiating elements. The given configuration of array is presented as shown by Fig. 2. The array factor $AF(\theta)$ obtained to optimize is considered by the author as follows.

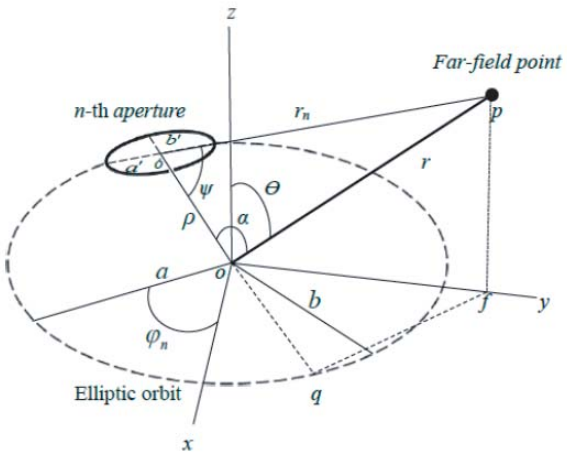

Figure 2. The geometry of elliptical apertures array.

The interest of this section first is to prove the approximate relation $r \cong r_n$ using the binomial theorem. The center of elliptic orbit in the spherical coordinates' origin is defined by o, where the distance between the centers of each aperture and elliptic orbit is denoted by ρ. According to the cosines law, the expressions shown by Equation (14) are applied to triangle $o\acute{o}p$.

$$\begin{aligned} r_n^2 &= r^2 + \rho^2 - 2\rho r\cos\alpha \\ r_n &= (r^2 + \rho^2 - 2\rho r\cos\alpha)^{\frac{1}{2}} \\ \frac{1}{r_n} &= \frac{1}{r}\left(1 + \frac{\rho^2}{r^2} - \frac{2\rho}{r}\cos\alpha\right)^{\frac{-1}{2}} \\ r^2 &\geq \rho^2 \\ \frac{1}{r_n} &\cong \frac{1}{r}\left(1 - \frac{2\rho}{r}\cos\alpha\right)^{\frac{-1}{2}} \cong \frac{1}{r}\left(1 + \frac{\rho}{r}\cos\alpha\right) \end{aligned} \tag{16}$$

The projection of r on the radius of and the projection of on oq as expressed are utilized to simplify Equation (14).

$$\begin{aligned} r\sin\theta &= of \\ of\cos\varphi = r\sin\theta\cos\varphi &= oq \\ oq = \rho &\Longrightarrow r\sin\theta\cos\varphi = \rho \end{aligned} \tag{17}$$

Using Equation (15) in (14) specifies the relation between r and r_n.

$$r \cong r_n(1 + \sin\theta\cos\varphi\cos\alpha) \tag{18}$$

The author applies a supposition to eliminate the trigonometric expression in Equation (16). By the assumption that $o\acute{o}p$ is a right triangle, $\alpha = \frac{\pi}{2}$ and $r \cong r_n$. With respect to the relation $r \cong r_n$, the distance between a point inside n_{th} aperture and the observation zone is computed from the elliptic orbit center. φ_n denotes the angular position of n_{th} aperture.

$$\begin{aligned} \acute{r_n} &= a\cos\varphi_n\hat{x} + b\sin\varphi_n\hat{y} \\ \hat{r}\cdot\acute{r_n} &= \sin\theta(a\cos\varphi\cos\varphi_n + b\sin\varphi\sin\varphi_n) \end{aligned} \tag{19}$$

Transform Equation (19) into spherical coordinates to obtain the elliptical orbit vector components on x-y plane, which are substituted in Equation (20):

$$\begin{aligned} &A_n = a\cos\varphi_n \quad B_n = b\sin\varphi_n \\ &A_n\cos\varphi + B_n\sin\varphi = C_n\cos(\delta_n - \varphi) \\ &C_n = (A_n^2 + B_n^2)\frac{1}{2} \quad \delta_n = \arctan\frac{B_n}{A_n} \end{aligned} \tag{20}$$

Hence Equation (17) is reduced to

$$\hat{r}\cdot\acute{r_n} = \sin\theta(C_n\cos(\delta_n - \varphi))$$

The calculation of n_{th} aperture electric far-field is by the supposition that the aperture is in a perfect electric conducting plane, and the electric field is x-directed. Sa represents the elliptical aperture area.

$$P_x = a_x E_i \iint_{Sa} e^{j\beta\hat{r}\acute{r}_n} d\acute{S} \tag{21}$$

Equation (19) becomes

$$P_x = a_x E_i 4\acute{a}\acute{b}\int_0^{\frac{\pi}{2}} e^{j\beta C_n\sin\theta\cos(\delta_n-\varphi)}\sin^2\varphi\, d\acute{\varphi} \tag{22}$$

The integral involving trigonometric function is written

$$P_x = a_x E_i 4\acute{a}\acute{b}\int_0^{\frac{\pi}{2}} e^{j\beta C_n\sin\theta\cos(\delta_n-\varphi)}\left(\frac{1-\cos 2\varphi}{2}\right) d\acute{\varphi} \tag{23}$$

The integral, true for finite values of φ in the interval $0-\frac{\pi}{2}$, is simplified to an expression involved in Bessel function. The author assigns $\lambda = (\beta C_n \sin\theta)$.

$$P_x = a_x E_i \pi \acute{a}\acute{b}\left(J_0(\lambda) + \Re e J_2(\lambda) e^{-j2\delta_n}\right) \tag{24}$$

J_0 is the Bessel function of the first kind of order null and J_2 the Bessel function of the first kind of order two.

$$P_x = a_x E_i \pi \acute{a}\acute{b}\left(J_0(\lambda) + \cos 2\delta_n J_2(\lambda)\right) \tag{25}$$

The calculation results of Equations (17)–(23) are shown below.
Using Equation (13)

$$\vec{E}_{n_t h(total)} = (\hat{\theta}\cos\varphi - \hat{\varphi}\cos\theta\sin\varphi) j\beta e^{-j\beta r} E_i \frac{\acute{a}\acute{b}}{2r}\left(J_0(\lambda) + \cos 2\delta_n J_2(\lambda)\right) \tag{26}$$

The vector of polarization:

$$\hat{p} = (\hat{\theta}\cos\varphi - \hat{\varphi}\cos\theta\sin\varphi)$$

Equation (24) is expanded to the all array elements by a series in intervals 1–10 subsequently to obtain the array factor.
The total electric far-field of array:

$$\vec{E}_{(total)} = \hat{p} j\beta e^{-j\beta r} E_i \frac{\acute{a}\acute{b}}{2r} \sum_{n=1}^{10}\left(J_0(\lambda) + \cos 2\delta_n J_2(\lambda)\right) \tag{27}$$

The electric far-field of array in the E-plane at $\varphi = 0$.

$$\vec{E}_\theta = \hat{\theta}\,\hat{p} j\beta e^{-j\beta r} E_i \frac{\acute{a}\acute{b}}{2r} \sum_{n=1}^{10}\left(J_0(\lambda) + \cos 2\delta_n J_2(\lambda)\right) \tag{28}$$

The array factor at $\theta = \theta_0 = 0$.

$$AF(\theta) = \sum_{n=1}^{10}\left(J_0(\lambda) + \cos 2\delta_n J_2(\lambda)\right) \tag{29}$$

The calculation of n_{th} aperture electric far-field is by the supposition that the aperture is in a perfect electric conducting plane, and the electric field is y-directed. Sa represents the elliptical aperture area.

$$P_y = a_y E_i \iint_{Sa} e^{j\beta\hat{r}\acute{r}_n} d\acute{S} \tag{30}$$

The computational manner is continued in the same way as considered in Equations (20)–(27).

$$P_y = a_y E_i 4\acute{a}\acute{b} \int_0^{\frac{\pi}{2}} e^{j\beta C_n \sin\theta\cos(\delta_n - \varphi)} \cos^2\varphi \, d\acute{\varphi} \tag{31}$$

$$P_y = a_y E_i 4\acute{a}\acute{b} \int_0^{\frac{\pi}{2}} e^{j\beta C_n \sin\theta\cos(\delta_n - \varphi)} \left(\frac{1+\cos 2\varphi}{2}\right) d\acute{\varphi} \tag{32}$$

Equation (29) is simplified to Equation (30) involved in Bessel function.

$$P_y = a_y E_i \pi \acute{a}\acute{b}\left(J_0(\lambda) - \Re e J_2(\lambda) e^{-j2\delta_n}\right) \tag{33}$$

The calculations results of Equations (29)–(31) are shown below.
Using Equation (13)

$$\vec{E}_{n_t h(total)} = (\hat{\theta}\sin\varphi + \hat{\varphi}\cos\theta\cos\varphi) j\beta e^{-j\beta r} E_i \frac{\acute{a}\acute{b}}{2r}\left(J_0(\lambda) - \cos 2\delta_n J_2(\lambda)\right) \tag{34}$$

The vector of polarization:

$$\hat{p} = (\hat{\theta}\sin\varphi + \hat{\varphi}\cos\theta\cos\varphi)$$

In order to obtain the array factor, Equation (34) is expanded to the all array elements by a series in the interval 1–10.

$$\vec{E}_{(total)} = \hat{p}j\beta e^{-j\beta r} E_i \frac{\acute{a}\acute{b}}{2r} \sum_{n=1}^{10} (J_0(\lambda) - \cos 2\delta_n J_2(\lambda)) \tag{35}$$

The electric far-field of array in the E-plane is at $\varphi = \frac{\pi}{2}$.

$$\vec{E}_\theta = \hat{\theta}\,\hat{p}j\beta e^{-j\beta r} E_i \frac{\acute{a}\acute{b}}{2r} \sum_{n=1}^{10} (J_0(\lambda) - \cos 2\delta_n J_2(\lambda)) \tag{36}$$

The array factor is at $\theta = \theta_0 = 0$.

$$AF(\theta) = \sum_{n=1}^{10} (J_0(\lambda) - \cos 2\delta_n J_2(\lambda)) \tag{37}$$

3. OPTIMIZATION METHOD

The pertinent parameters (eccentricity and angular positions of each element) excited to obtain the specified radiation characteristics of antenna array are determined through the geometric computational technique (GCT) in amalgamation with APE. In this work, the optimization process progresses gradually.

In the leading phase, solely for the advantage of the GCT, determine the optimal eccentricity value, and afterwards in the case of non-attainment of privileged status of the radiation pattern, apply the APE to excite the angular position of each array element.

This article pursues the desirable methodical optimization, whose authenticity is ascertained by the determined efficacious amounts of excited parameters led to obtaining the low SLL array pattern with high directivity.

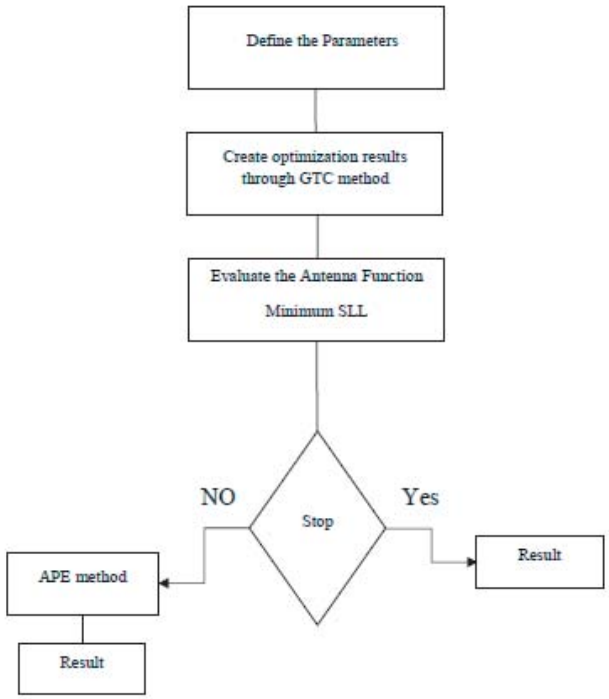

Figure 3. Basic scheme for optimization method.

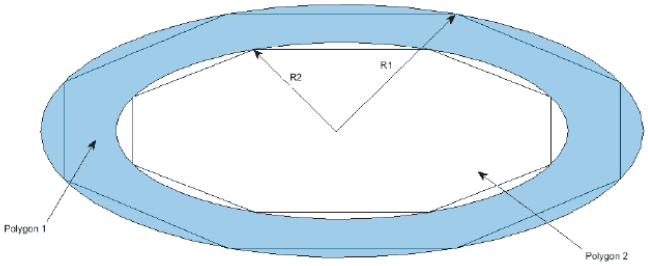

Figure 4. Geometric diagram.

3.1. Geometric Computational Technique (GCT)

The GCT in the framework of an optimization algorithm and presented as a coherent innovative manner by the author has significant conformity with desired antenna array configuration. The GCT endeavors to find an optimal quantity of the eccentricity. The space of searching illustrated in Fig. 4 is confined to a geometric diagram obtained by number of concentric ellipses, each of which inscribes one rectangle with geometric characteristics. Referring to the paragraph in the introduction, the sequence of rectangles inside the oval zones also yields two polygons. As mentioned by calculating area of the space between two created polygons, the attainment of the acquired equation as the essential function to obtain the eligible amount of eccentricity is procurable. The calculation of desired equation is dependent on number of polygons sides and the measurement of semi- and major-axes inside desired geometric zone. Accordingly, the process of proliferation quantitatively to increase the number of concentric ellipses in the both diagram zones is accomplished by including the $\frac{\pi}{j}$ phase difference between intersecting ellipses. Despite the phase difference between intersecting ellipses, the sides measure of each rectangle compared to its intersecting one is obtained based on a mathematical map relying on the differentiation method. The sides of inscribed rectangles equated to x and y components of each ellipse are depicted by the parametric equations to facilitate the area computational method of the space between two polygons. The GCT procedure at the commencement is in quest to acquire the area equation of the space between created polygons. The obtained equation comprises two substantial parameters, whole number of polygons sides in the geometric diagram zones plus the numeric ratio among the semi-major and semi-minor axes of two proliferated concentric ellipses. The alterations in the aforementioned parameters accomplished by the consecutive iterations eventually result in the most acceptable quantity of eccentricity at the order of iterations. The GCT is briefly explainable by the convenient expression of mathematics as stated below.

$$\Lambda_{Polygon1} - \Lambda_{Polygon2} = \varsigma_{space} \tag{38}$$

$$N \sin\varphi (R_{ellipse1} - R_{ellipse2}) = \varsigma_{space} \tag{39}$$

$$R_{ellipse2} = \frac{Mh \sin\delta}{N \sin\varphi} \frac{m+1}{m^2-1} \tag{40}$$

$$Eccentricity = \lim_{m \longrightarrow x} \sqrt{\frac{m^2-1}{m^2}} \tag{41}$$

In the above equations, $\Lambda_{Polygon1}$ defines the area of bigger polygon, while $\Lambda_{Polygon2}$ is the area of smaller one. N represents the number of polygons sides. $R_{ellipse1}$ and $R_{ellipse2}$ describe in order radius of bigger and smaller ellipses in geometric diagram. m is the numeric difference among the semi and major axes. h in Equation (38) is illustrated as the height of created Trapezoids in space between two polygons, where M involves in equation in order to explain the number of trapezoidal areas. In the following optimization procedure, we allocate affiliated utilized components in the above equations to excite. The excited parameters include the number of polygons sides, the numeric difference among the ellipses axes, and the element of h, which as defined will vary by axes excitation. The generating

processes will be done continuously until the solution meets the best target amount after consecutive iterations to attain the eligible quantity of eccentricity.

Explained by the flowchart in Fig. 3, if eccentricity excitation does not attain desired low SLL, we will commence the second step of optimization, processed by APE to excite the angular positions. The request is a Side Lobe Level parameter in the measure of $SLL \leq -17\,\mathrm{dB}$

$$AF = \sum_{num=1}^{Num} F_{num}(\chi_{num})$$

$$F_{num}(\chi_{num}) = J_0(\chi_{num}) \pm \zeta J_2(\chi_{num})$$

$$subject\ to\ \varphi_{num}\ \in\ \chi_{num}$$

$$AF = \prod_{num}^{Num} J_0(\varphi_{num}) \pm \zeta J_2(\varphi_{num})$$

$$leads\ to\ minimize\ SLL \leq -15\,\mathrm{dB}$$

$$If\ AF(\varphi_{num}optimum) < AF(\varphi_{num})$$

$$\varphi_{num} = g(r)\ and\ r\ known\ as\ ellipse\ radius,\ where\ x_{num} = r\cos(\varphi_{num})$$

$$\Downarrow$$

$$g(r) = \varphi_{num} = \arccos\left(\frac{a}{(a^2+b^2)\left(2 - \dfrac{num}{Num}\right)}\right)$$

$$num,\ number\ of\ n_{nth}\ \ element,\ Num,\ total\ number\ of\ array\ components$$

In the following, some computer simulations are conducted to verify the validation of the proposed method. We consider elliptical aperture antenna array with 10 elements, where the operating frequency illustrates the measure of 2 GHz. Some examples were simulated to demonstrate the performance of GCT and APE methods. Figs. 5 and 6 show the normalized unmodified patterns of the antenna array with non-attained level of side lobes compared to main beam.

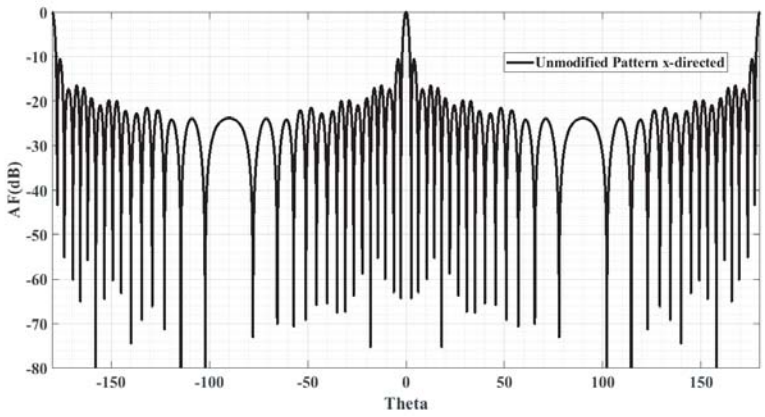

Figure 5. Unmodified pattern at x-directed field; $Frequency = 2\,\mathrm{GHz}$, $SLL = -10.64\,\mathrm{dB}$, $FNBW = 5.2^\circ$, $Num = 10$, $Eccentricity = 0.8660$.

Tables 1 and 2 contain the details of unmodified states numerical results, whose measurements by defined optimization manner of article need to be optimized. The determined antenna array function is mathematically obtained to accurately simulate radiation pattern in dB scale by Matlab code, while the HFSS software also facilitated simulations to receive the radiation parameters such as Directivity and Gain associated with Matlab computational responses.

The simulations in same condition are created, and 2 GHz operating frequency is assigned for them to run. All steps of simulations first have been done by Matlab and then will be processed by HFSS in

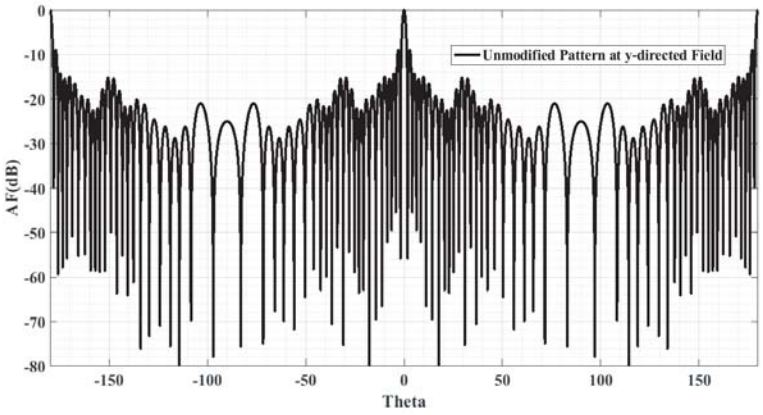

Figure 6. Unmodified pattern at y-directed field; $Frequency = 2\,\text{GHz}$, $SLL = -8.97\,\text{dB}$, $FNBW = 3.7^\circ$, $Num = 10$, $Eccentricity = 0.8660$.

Table 1. Unmodified patterns, x-directed field pattern.

Num	10
Eccentricity	0.866
m	2
SLL	$-10.64\,\text{dB}$
FNBW (Degree)	5.2

Table 2. Unmodified patterns, y-directed field pattern.

Num	10
Eccentricity	0.866
m	2
SLL	$-8.97\,\text{dB}$
FNBW (Degree)	3.7

3D scale. The author illustrated the variations of radiation parameters of antenna in previous articles via number of code sentences, whose method has been converted to integration of Matlab software with HFSS computational tools.

In order to study the behavior of utilized GCT and APE, the author compares the performance of optimization procedure with utilized algorithms in an article written by Sharaqa and Dib [12] to confirm the accuracy and competence of determined results of our work.

We assigned the especial way using MATLAB for synthesis of the antenna array pattern with the desired values of the proposed antenna parameters to reduce array SLL utilized by GCT and in the second step via explained APE manner to excite angular positions of the antenna elements, which obtain appropriate results after consecutive iterations.

The needed number of iterations to determine the acceptable outcomes is 1000–2000. The reached values of results demonstrated by simulations will be investigated and presented in two different modes for an elliptical antenna array composed of 10 uniform elliptical apertures as the radiating elements at x and y-directed field patterns.

The array function will be constructed for maximizing the SLL reduction with high directivity as well as receiving the outstanding eccentricity value of antenna array orbit, which is associated with optimized radiation parameters leading to SLL reduction and high directivity for each directional beam steering.

The excitation angular positions for each antenna element is constrained to lie between 0 and 2π only for y-directed mode. The obtained results will be computed as given in Tables plus simulated by HFSS software as shown as follows.

The states of array antenna patterns at $\varphi_0 = 90$ and $\varphi_0 = 0$ in this section can provide the best conditions for elliptical aperture array patterns indicated in Tables 3 and 4.

Table 3. x-directed patterns, comparison between algorithms.

Algorithm	GCT	SADE	BBO	FA
Eccentricity	0.9922	0.9922	0.9922	0.9922
major-axis	5.6249	5.6249	5.6249	5.6249
minor-axis	0.5114	0.5114	0.5114	0.5114
Num	10	10	10	10
SLL	−23.55 dB	−23 dB	−17.8 dB	−15.3 dB
FNBW (Degree)	5.6	8.2	6.2	8.7

Table 4. y-directed patterns, comparison between algorithms.

Algorithm	GCT and APE	SADE	BBO	FA
Eccentricity	0.8760	0.8760	0.8760	0.8760
major-axis	4.2099	4.2099	4.2099	4.2099
minor-axis	2.1049	2.1049	2.1049	2.1049
Num	10	10	10	10
SLL	−17.08 dB	−13.65 dB	−11 dB	−13.7 dB
FNBW (Degree)	8.4	7	10	3.6

Figs. 7–8 as presented as follows obtained after 2000 iterations show the ability of GCT method to improve the antenna array pattern in angle $\varphi_0 = 0$ at x-directed mode with good radiation parameters' values such as the side lobe level, directivity, and main pattern beamwidth in comparison with other algorithms. The optimization of array signal at y-directed state will be accomplished and finalized via integration of GCT and APE processed in two steps of optimization method and also compared with used algorithms in [12].

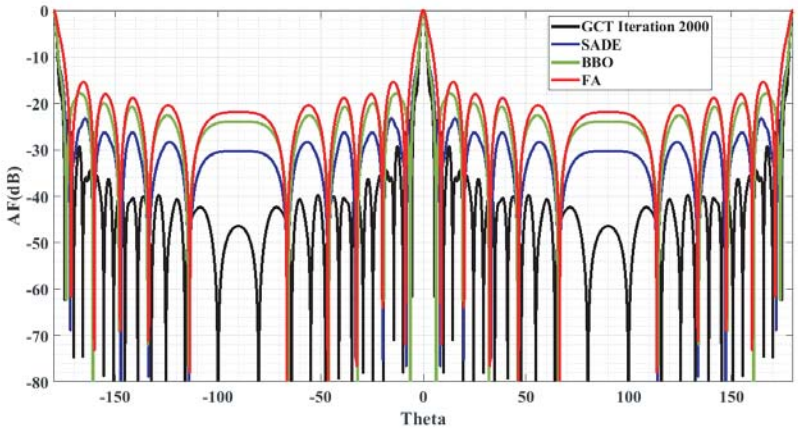

Figure 7. 10 Element-elliptical aperture array comparison of algorithms, $\varphi_0 = 0$, *Operating Frequency* = 2 GHz. x-directed field.

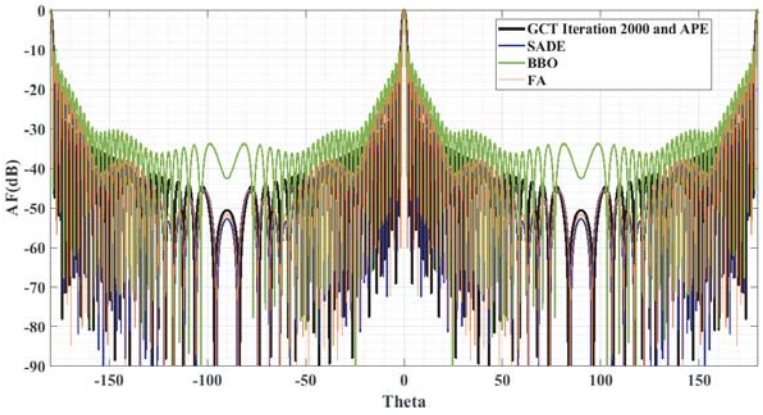

Figure 8. 10 Element-elliptical aperture array comparison of algorithms, $\varphi_0 = 90$, *Operating Frequency* $= 2$ GHz. y-directed field.

Best values consisting last modified iterations and compared outcomes have been shown and discussed in Tables 3.

In this table, the values of FNBW and the SLL using GCT and optimization methods in [12] for x-directed array patterns at $\varphi_0 = 0$ are illustrated, which is shown in in Fig. 7 at $\varphi_0 = 0$. The best value of FNBW for an x-directed 10-element array is 5.6 degrees, and the best SLL using GCT is -23.55 dB (2000th iteration).

In another mode, Fig. 8 shows a 10-element y-directed elliptical aperture array pattern with modified values of radiation parameters at $\varphi_0 = 90$ by GCT, APE against compared algorithms. In order to obtain the best values for the 10-element y-directed array, as mentioned the optimization method also has to be processed by the second step including angular position excitation, which results in the suitable measure of desired parameters.

We analyzed the numerical results from the simulated structures of the antenna patterns, and finally we found that the final states (2000th iteration) present better computed results with maximum reduction in SLL than unmodified status and compared algorithms results. Hence, we can introduce them as the states optimized propagation in Figs. 9–10.

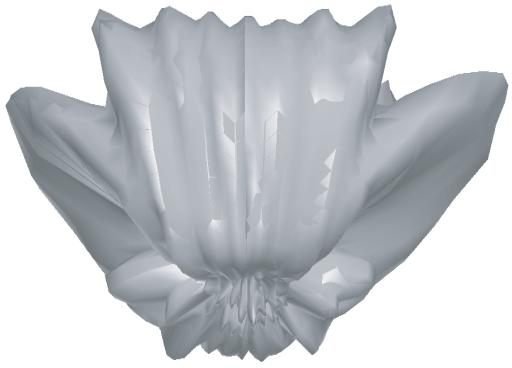

Figure 9. 10 Element-elliptical aperture array, *Operating Frequency* $= 2$ GHz. x-directed field.

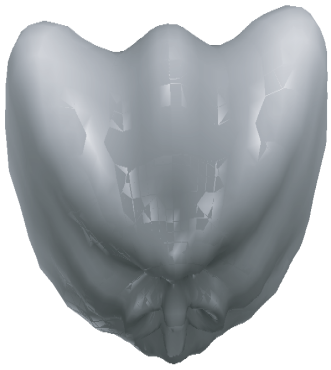

Figure 10. 10 Element-elliptical aperture array, *Operating Frequency* $= 2$ GHz. y-directed field.

In the tables, the values of directivity, gain and the SLL using GCT and APE are demonstrated for x-directed field pattern at $\varphi_0 = 0$ and y-directed field at $\varphi_0 = 90$. The best values of directivity, gain and SLL, respectively, for x-directed field pattern at $\varphi_0 = 0$ and y-directed field pattern at $\varphi_0 = 90$ (2000th iteration) in order are -23.55 dB and -17.8 dB.

The methods of GCT and APE present a acceptable performance in terms of the SLL with respect to designed antenna array structure and maintain the values of directivity and gain. In the performance of these optimization methods, the results of the measured radiation parameters for the optimized design are really outstanding. These values mean a substantial improvement in the behavior of the new array antenna for the design. The method of GCT and APE, with respect to the conventional case of progressive compared algorithms, present substantial improvements obtained in the sense of the SLL, directivity, and gain and seen to give radiation patterns, which are generally determined by a coherent innovative manner detailed in Tables 5–6.

Table 5. Modified pattern, radiation parameters of best determined states.

Iteration2000	GCT
SLL	−23.55 dB
Directivity	8.95 dB
Gain	7.3833 dB

Table 6. Modified pattern, radiation parameters of best determined states.

Iteration2000	GCT and APE
SLL	−17.8 dB
Directivity	5.3909 dB
Gain	5.2115 dB

4. CONCLUSION

In this paper, GCT and APE are used to obtain maximum reduction in side lobe level relative to improve the directivity. The GCT method associated with APE was used to determine the eligible antenna parameters with elliptical aperture array to optimize the antenna pattern. This method is very effective and can be utilized in practice to synthesize other structures. All these factors together have been considered for optimal results in our design problem, and they account for the understatement of the author's work.

REFERENCES

1. Stutzman, W. L. and G. A. Thiele, *Antenna Theory and Design*, John Wiley and Sons, 1996.
2. Saman Zare, A., "Elliptical antenna array pattern synthesis with fixed side lobe level and suitable main beam width by genetic algorithm," *Progress in American Journal of Electromagnetics and Applications*, Vol. 1, No. 1, 8–15, 2013.
3. Cheng, D. K., *Field and Wave Electromagnetics*, Adison Wesley, 1983.
4. Saman Zare, A., "Application of ant colony optimization algorithm to pattern synthesis of uniform circular antenna array," *Progress in ACES Journal*, Vol. 30, No. 8, 810–818, 2015.
5. Balanis, C. A., *Antenna Theory Analysis and Design*, John Wiley and Sons, 2011.
6. Bevelacqua, P. J., "Antenna arrays-performance limits and geometry," Doctoral Thesis, Virginia Tech. University, Antenna Engineering Team, 2007.
7. Zaharis, Z. D., C. Skeberis, and T. D. Xenos, "Improved antenna array adaptive beamforming with low side lobe level using a novel adaptive invasive weed optimization method," *Progress In Electromagnetics Research*, Vol. 124, 137–150, 2012.
8. Mahanti, G. K., A. Chakrabarty, and S. Das, "Phase-only and amplitude-phase only synthesis of dual-beam pattern linear antenna arrays using floating-point genetic algorithms," *Progress In Electromagnetics Research*, Vol. 68, 247–259, 2007.

9. Guney, K. and M. Onay, "Amplitude-only pattern nulling of linear antenna arrays with the use of bees algorithm," *Progress In Electromagnetics Research*, Vol. 70, 21–36, 2007.
10. Dessouky, M. I., H. A. Sharshar, and Y. A. Albagory, "Efficient sidelobe reduction technique for small-sized concentric circular arrays," *Progress In Electromagnetics Research*, Vol. 65, 187–200, 2006.
11. Manica, L., P. Rocca, M. Pastorino, and A. Massa, "Boresight slope optimization of subarrayed linear arrays through the contiguous partition method," *IEEE Antennas Wireless Propag. Lett.*, Vol. 8, 253–257, 2008.
12. Sharaqa, A. and N. Dib, "Position-only side lobe reduction of a uniformly excited elliptical antenna array using evolutionary algorithms," *IET Microwaves, Antenna and Propagation*, Vol. 7, No. 6, 452–457, Apr. 23, 2013.
13. Liu, D., Q. Feng, W.-B. Wang, and X. Yu, "Synthesis of unequally spaced antenna arrays by using inheritance learning particle swarm optimization," *Progress In Electromagnetics Research*, Vol. 118, 205–221, 2011.
14. Dolph, C. L., "A current distribution for broadside arrays which optimises the relationship between beam width and sidelobe level," *IRE Proc.*, Vol. 34, 335–348, 1946.
15. Saman Zare, A., "Elliptical antenna array pattern synthesis with fixed side lobe level and suitable main beam width by genetic algorithm," *Progress in Majlesi Journal of Telecommunications Devices*, Vol. 1, No. 4, 113–120, 2012.
16. Saman Zare, A., "Elliptical antenna array pattern synthesis," B.S.C. Thesis, Islamic Azad University Majlesi Branch, Telecommunications Engineering Department, 2012.
17. Targonski, S. D., R. B. Waterhouse, and D. M. Pozar, "Wide-band aperture-coupled stacked patch antenna using thick substrate," *Electron. Lett.*, Vol. 32, No. 21, 1941–1942, Nov. 1996.
18. Munson, R. E., "Conformal microstrip antennas and microstrip phased arrays," *IEEE Trans. Antennas and Propagat.*, Vol. 22, No. 1, 74–78, Jan. 1974.
19. Lei, J.-Z., C.-H. Liang, W. Ding, and Y. Zhang, "EMC analysis of antennas mounted on electrically large platforms with parallel FDTD method," *Progress In Electromagnetics Research*, Vol. 84, 205–220, 2008.
20. Gurel, L. and O. Ergul, "Design and simulation of circular arrays of trapezoidal-tooth log-periodic antennas via genetic optimization," *Progress In Electromagnetics Research*, Vol. 85, 243–260, 2008.